
Real-Time Regression with Dividing Local Gaussian Processes

Armin Lederer

Technical University of Munich
80333 Munich, Germany
armin.lederer@tum.de

Alejandro José Ordóñez Conejo

Tecnológico de Costa Rica
30101 Cartago, Costa Rica
ajoseoc@gmail.com

Korbinian Maier

FRANKA EMIKA GmbH
80797 Munich, Germany
korbinian.maier@franka.de

Wenxin Xiao

Peking University
100871 Beijing, China
xiao.wenxin@foxmail.com

Jonas Umlauft

Technical University of Munich
80333 Munich, Germany
jonas.umlauf@tum.de

Sandra Hirche

Technical University of Munich
80333 Munich, Germany
hirche@tum.de

Abstract

The increased demand for online prediction and the growing availability of large data sets drives the need for computationally efficient models. While exact Gaussian process regression shows various favorable theoretical properties (uncertainty estimate, unlimited expressive power), the poor scaling with respect to the training set size prohibits its application in big data regimes in real-time. Therefore, this paper proposes dividing local Gaussian processes, which are a novel, computationally efficient modeling approach based on Gaussian process regression. Due to an iterative, data-driven division of the input space, they achieve a sublinear computational complexity in the total number of training points in practice, while providing excellent predictive distributions. A numerical evaluation on real-world data sets shows their advantages over other state-of-the-art methods in terms of accuracy as well as prediction and update speed.

1 Introduction

Recent technological trends enable ever growing storage capacities and declining costs for sensor hardware, resulting in a significant increase of available data, which allows for in-depth analysis and precise modeling of various technical systems. As the amount of data increases, it becomes inevitable to design methods which scale well to large data sets. Especially in control applications, scalability is additionally constrained by high update rates and real-time requirements on the prediction. These applications include the control of autonomous cars, unmanned aerial vehicles [1], robotic manipulators [2], combustion engines [3, 4] and many others, where update rates in the magnitude of 10^2 Hz to 10^4 Hz are required. In case of predictive control schemes, where possible future trajectories are inferred and evaluated, multiple predictions are made for a single control command, requiring prediction rates, which are orders of magnitudes higher [5].

Parametric learning approaches transfer all information from the data into parameters and therefore typically have constant computational complexity of predictions and updates independent of the

number of data points [6]. While this generally allows real-time regression, it comes at the cost of limited model flexibility and requires expert knowledge. In contrast, non-parametric learning methods such as Gaussian processes (GPs) can provide unlimited expressive power [7], but grow in complexity with the number of training points. Therefore, they suffer from increasing prediction and update times. In order to mitigate this issue, several approaches have focused on reducing the complexity of posterior mean computations, such as, e.g., inducing point methods [2, 8] or deterministic training conditional approximations [9, 10]. However, allowing model updates in real-time has attracted far less attention, and the quality of predictive distributions in online regression has barely been addressed.

The main contribution of this paper is a novel, computationally efficient, GP-based method for real-time predictions and model updates, called dividing local Gaussian process (DLGP). Our approach is based on an online, data-driven division of the input space in order to build local GP models. The division of the data during training, and the combination of local models for prediction are both performed with a sublinear computational complexity in practice. In a numerical study, we compare our approach with existing state-of-the-art modeling techniques on real-world data sets with respect to training and prediction time as well as prediction error and quality of the predictive distributions. The paper is structured as follows: In Section 2, we discuss the related work in depth and briefly introduce GP regression. Section 3 presents the proposed DLGP model and in Section 4 the numerical results are compared.

2 Background

2.1 Related Work

Real-time regression for data-driven models is a challenge that has originally been considered in the context of robotics [6], and recently it gains increasing attention in control theory [11] and reinforcement learning [12]. In early work, this problem has been approached by adapting existing non-parametric methods, such as support vector regression [13], to enable real-time learning. Due to computational limitations, this approach is difficult to apply in practice. This lead to the development of dedicated real-time learning methods based on linear regression, which are typically referred to as locally weighted projection regression (LWPR) [14, 15]. LWPR owes its success to reasonable regression quality, high update and prediction rates, and its straightforward usage with publicly available software [16]. Due to these reasons, it is commonly applied in robotics [17, 18] and control [19] up to today. However, the regression quality of LWPR significantly depends on design parameters, which require careful tuning in practice, and therefore contradicts the online learning paradigm. In order to overcome this issue, Bayesian adaptations of LWPR have been proposed, which base on variational inference [20, 21], and novel methods using mean field variational Bayesian approximate inference have been developed [22]. Despite of their theoretical advantages, these methods can barely be found in applications.

In recent years, Gaussian process approximations have experienced a great success in online regression research due to the straightforward update rules originating from Bayes theory. Due to the high computational complexity of exact updates, a large variety of strategies has been developed to mitigate this issue. Originally developed for large data sets [23], sparse methods have been among the first to be applied to real-time learning [24]. Some methods use deterministic training conditional approximations with active subsets of the training data, which are determined using different metrics [24, 2, 8, 25], while others achieve sparsity by using inducing points chosen online [9, 10, 26], or through compactified covariance functions resulting in sparse cholesky factors [27, 28]. Alternative approaches rely on variational inference based on the free energy approximation [29] or solve variational inference in the reproducing kernel Hilbert space via stochastic mirror descent [30] to deal with streaming data online. Although these approaches can achieve a small prediction error with sufficiently many inducing points, their updates for new training data are rather slow. When choosing a small number of inducing points to reduce the update time, the prediction performance of these methods typically drops significantly. This is due to the fact that a lot of information from the training data cannot be included into the model, which significantly limits the asymptotic performance of such approaches. Using explicit features and parametric learning can mitigate these problems. In particular, when offline data is available, the features can be fitted to this data using neural networks [31] or least squares [32]. Conversely, without any offline data, random trigonometric features with strong theoretical guarantees can be easily determined using Bochner's theorem [33], leading to the

method's name sparse spectrum GP [34]. These methods are known to suffer from overfitting [35] and their posterior variances are overconfident [36]. Furthermore, the posterior mean and variance will be periodic functions, such that the variance might collapse far from any training samples [37] leading to overconfident predictions. In contrast to sparse likelihood approximations and kernel approximations, Local GP methods [38] follow a different idea: By combining the predictions of multiple GP models, the overall computational complexity is reduced. The usage of multiple GPs is typically exploited by spatially separating them, which is usually referred to as local GPs [39, 40], although random training point assignment to models also allows real-time regression [41]. A similar effect can be achieved using a single GP with moving window to select training samples [42]. Since the complexity of exact inference in local models still leads to quickly growing computational complexity, this is typically avoided by using sparse local GPs, inheriting many of the disadvantages. Therefore, we pursue a different approach by dividing data sets and retraining the local models when they become too large. Thereby, we reduce computational complexity of predictions and updates, without suffering from the disadvantages of sparse GP approximations.

2.2 Gaussian Processes Regression

A Gaussian process \mathcal{GP} is the generalization of a Gaussian distribution, and bases on the assumption that any finite collection of random variables $y_i \in \mathbb{R}$ follows a joint Gaussian distribution. This joint Gaussian distribution is uniquely defined by the prior mean, which is frequently set to 0, and a covariance function $k : \mathbb{R}^d \times \mathbb{R}^d \rightarrow \mathbb{R}$ [7]. The observations y_i can be considered as measurements of a sample function $f : \mathbb{R}^d \rightarrow \mathbb{R}$ of the GP distribution and are typically perturbed by zero mean Gaussian noise with variance $\sigma_n^2 \in \mathbb{R}_{+,0}$. We concatenate N input training samples \mathbf{x}_i and output observations y_i into a matrix \mathbf{X} and a vector \mathbf{y} , which represent the training data set \mathbb{D} . Furthermore, we define the elements of the GP kernel matrix $\mathbf{K}(\mathbf{X}, \mathbf{X})$ as $K_{ij} = k(\mathbf{x}_i, \mathbf{x}_j)$ and define the elements of the kernel vector $\mathbf{k}(\mathbf{X}, \mathbf{x})$ accordingly. Based on these definitions, we can represent the GP model efficiently as

$$\mathbf{L} = \text{cholesky}(\mathbf{K}(\mathbf{X}, \mathbf{X}) + \sigma_n^2 \mathbf{I}) \quad \boldsymbol{\alpha} = \mathbf{L}^T \setminus (\mathbf{L} \setminus \mathbf{y}) \quad (1)$$

where " \setminus " denotes the forward and backward substitution, respectively, such that $\mathcal{O}(N^3)$ and $\mathcal{O}(N^2)$ operations are required for the computation of \mathbf{L} and $\boldsymbol{\alpha}$ [7], respectively. Then, the posterior GP distribution $p_{\mathcal{GP}}(f(\mathbf{x})|\mathbf{x}, \mathbb{D}) = \mathcal{N}(\mu(\mathbf{x}), \sigma^2(\mathbf{x}))$ at a test point \mathbf{x} can be computed using

$$\mu(\mathbf{x}) = \mathbf{k}(\mathbf{X}, \mathbf{x}) \boldsymbol{\alpha} \quad \mathbf{v} = \mathbf{L} \setminus \mathbf{k}(\mathbf{X}, \mathbf{x}) \quad \sigma^2(\mathbf{x}) = k(\mathbf{x}, \mathbf{x}) - \mathbf{v}^T \mathbf{v}, \quad (2)$$

which requires $\mathcal{O}(N)$ and $\mathcal{O}(N^2)$ calculations for the posterior mean and variance, respectively [7].

3 Dividing Local Gaussian Processes

While existing local GP approaches for real-time learning base on the principle that all local models have the same spatial extension in the input domain, our proposed DLGP approach follows a different paradigm. Starting from a single, global model, local models are iteratively generated by dividing existing models. This is efficiently performed by sampling the data set, to which each training sample is assigned, from localizing random distributions. We explain this iterative binary tree construction using random data assignment in detail in Section 3.1. In Section 3.2, the combination of tree structure and localizing probability functions is exploited to derive analytical predictive distributions of the DLGP model.

3.1 Binary Tree Construction Using Probabilistic Training Data Assignment

Since we consider the problem of real-time regression, we have to deal with streaming data, i.e., sequentially arriving data samples. Therefore, we iteratively construct a model, starting with a single data set $\mathbb{D}_0 = \emptyset$. This data set constitutes the root node 0 of a binary tree T_{DLGP} , as depicted in Fig. 1. The incoming training data is added to the data set \mathbb{D}_0 , and each new data point can be efficiently included into the GP model (1) using rank one updates, which exhibit quadratic complexity [40]. When the number of training samples reaches a prescribed threshold \bar{N} , we extend the tree T_{DLGP} by growing leaf nodes 1, 2 with data sets $\mathbb{D}_1, \mathbb{D}_2$ as children of the root node 0, as shown in the center of Fig. 1. In order to distribute the data efficiently to the sets $\mathbb{D}_1, \mathbb{D}_2$, we define a function $p_0 : \mathbb{R}^d \rightarrow [0, 1]$, which returns the probability of an assignment of a point $\mathbf{x} \in \mathbb{R}^d$ to the

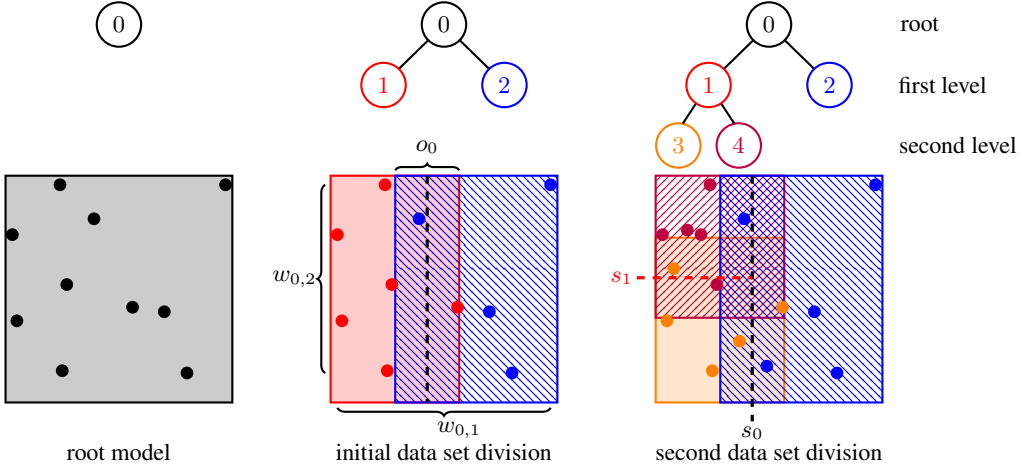


Figure 1: Iterative model tree construction and corresponding layout of the input space: active regions and training samples belonging to the same node are depicted in the same color.

set \mathbb{D}_1 , i.e., $P(\mathbf{x} \in \mathbb{D}_1 | \mathbf{x}) = p_0(\mathbf{x})$. We determine the probability $p_0(\mathbf{x})$ for each data pair (\mathbf{x}, y) in \mathbb{D}_0 , and sample the child node i from the corresponding Bernoulli distributions. After the data set division, we compute the local GP models (1) for both data sets, which generally has a complexity of $\mathcal{O}(\bar{N}^3)$ [7]. Note that the root node contains neither data nor a local GP model after the data set division, but instead encodes the structure of the data distribution using the function $p_0(\cdot)$. Therefore, $p_0(\cdot)$ is a crucial design choice of the DLGP algorithm. While we propose to use a function $p_0(\cdot)$ which causes a spatial division of the input space to exploit the locality of models during prediction as explained in Section 3.2, arbitrary choices are possible in general. An example of a spatial data set division is depicted in the center of Fig. 1.

After the initial data set division, we continue to assign the streaming data pairs (\mathbf{x}, y) to the sets $\mathbb{D}_1, \mathbb{D}_2$ by sampling from the Bernoulli distributions with parameters $p_0(\mathbf{x})$. When either of the sets $\mathbb{D}_1, \mathbb{D}_2$ reaches its data capacity limit \bar{N} , we define a new function $p_i(\cdot)$, $i = 1, 2$, which induces the conditional probability given the parent node, e.g., $P(\mathbf{x} \in \mathbb{D}_3 | \mathbf{x} \in \mathbb{D}_1, \mathbf{x}) = p_1(\mathbf{x})$. Based on this conditional probability, we repeat the division process as explained for the root node. Therefore, we add another level to the binary tree as shown on the right-hand side of Fig. 1. For further training data assignment, it is necessary to iteratively determine a branch of the binary tree using random transitions based on Bernoulli distributions with probability parameters $p_i(\mathbf{x})$ until a leaf node is reached, as outlined in Algorithm 1. Due to this random branch sampling, the computational complexity of updating the DLGP model strongly depends on the structure of the binary tree T_{DLGP} , which in turn is a result of the distribution and the order of the input training data \mathbf{x} . This leads to a worst case complexity of $\mathcal{O}(N + \bar{N}^3)$ for model updates, although in many cases, e.g., for uniformly distributed input training samples, we can achieve a lower complexity of $\mathcal{O}(\log(N) + \bar{N}^3)$ with a balanced tree.

3.2 Predictive Distribution

Since the training data is assigned through random sampling, predictive distributions of a DLGP can be calculated for test points without any further approximation. Due to the binary tree structure and the fact that all local models are in leaf nodes, this computation is straightforward: given the binary tree, we determine the set of leaf nodes \mathbb{I} . For each leaf $j \in \mathbb{I}$ with depth ν_j , we compute the marginal probability $\tilde{p}_j(\mathbf{x}) = P(\mathbb{D}_j | \mathbf{x})$ of the leaf node by multiplying the conditional probabilities $p_i(\mathbf{x})$ along its branch, i.e.,

$$\tilde{p}_j(\mathbf{x}) = \prod_{i=1}^{\nu_j} p_{\lfloor \frac{j+1}{2^i} \rfloor - 1}(\mathbf{x}). \quad (3)$$

By employing the definition of conditional probabilities, we obtain the predictive distribution

$$p_{\text{DLGP}}(f(\mathbf{x}) | \mathbf{x}, \mathbf{X}, \mathbf{y}) = \sum_{j \in \mathbb{I}} \tilde{p}_j(\mathbf{x}) p_{GP_j}(f(\mathbf{x}) | \mathbf{x}, \mathbb{D}_j), \quad (4)$$

Algorithm 1 Updating the DLGP model

```

1: function UPDATE( $T_{\text{DLGP}}$ ,  $\mathbf{x}, y$ )
2:    $i \leftarrow T_{\text{DLGP}}.\text{ROOT}()$ 
3:   while  $\neg \text{ISLEAF}(i)$  do ▷ random branch sampling
4:      $i \leftarrow i.\text{GETCHILD}(\text{DRAWBERNOULLI}(p_i(\mathbf{x})))$ 
5:   if  $|\mathbb{D}_i| = \bar{N}$  then ▷ decision about data set division
6:      $i.\text{GENERATECHILDREN}()$ 
7:   for each  $(\mathbf{x}', y') \in \mathbb{D}_i$  do ▷ random training set division
8:      $j \leftarrow i.\text{GETCHILD}(\text{DRAWBERNOULLI}(p_i(\mathbf{x}')))$ 
9:      $j.\text{ADDTODATASET}(\mathbf{x}', y')$ 
10:     $i.\text{LEFTCHILD}().\text{COMPUTELOCALGP}()$  ▷ re-computation of the GP models (1)
11:     $i.\text{RIGHTCHILD}().\text{COMPUTELOCALGP}()$ 
12:     $i \leftarrow i.\text{GETCHILD}(\text{DRAWBERNOULLI}(p_i(\mathbf{x})))$ 
13:    $i.\text{ADDTODATASET}(\mathbf{x}, y)$  ▷ random assignment of new data pair
14:    $i.\text{UPDATELOCALGP}()$  ▷ update of the GP model (1)
15: return  $T_{\text{DLGP}}$ 

```

where $p_{\mathcal{GP}_j}(f(\mathbf{x})|\mathbf{x}, \mathbb{D}_j)$ are the distributions of the local Gaussian processes \mathcal{GP}_j with posterior mean $\mu_j(\mathbf{x})$ and variance $\sigma_j^2(\mathbf{x})$, which can be computed with a complexity of $\mathcal{O}(\bar{N})$ and $\mathcal{O}(\bar{N}^2)$, respectively, using (2). The predictions of all local models are independent of each other, and therefore allow efficient parallelization. Moreover, from an ensemble point of view, the mean and variance functions of the predictive distribution $p_{\text{DLGP}}(f(\mathbf{x})|\mathbf{x}, \mathbf{X}, \mathbf{y})$ straightforwardly follow as

$$\mu_{\text{DLGP}}(\mathbf{x}) = \sum_{j \in \mathbb{I}} \tilde{p}_j(\mathbf{x}) \mu_j(\mathbf{x}) \quad (5)$$

$$\sigma_{\text{DLGP}}^2(\mathbf{x}) = \sum_{j \in \mathbb{I}} \tilde{p}_j(\mathbf{x}) (\sigma_j^2(\mathbf{x}) + \mu_j^2(\mathbf{x})) - \mu_{\text{DLGP}}^2(\mathbf{x}). \quad (6)$$

Therefore, DLGPs provide a stochastically sound framework for the computation of the predictive mean and variance function, and do not require further approximation like similar approaches such as, e.g., [38, 40]. While these local GP methods can set an upper bound on the number of models, which are used for prediction, this number grows indefinitely in DLGPs due to the continuous division of the local data sets. Since the computational complexity of a prediction grows with the number of local models used for prediction, we can trivially bound it by $\mathcal{O}(N\bar{N})$ for the mean and $\mathcal{O}(N\bar{N}^2)$ for the variance prediction.

In order to take advantage of the data set division in the predictions as well, we want the probabilities $p_i(\cdot)$ to spatially divide the input domain, such that in large regions of the input space only a single model is active by having a positive marginal probability $\tilde{p}_j(\mathbf{x})$, while there is merely a small overlapping region, in which multiple models are active. For this purpose, we employ probability functions $p_i(\cdot)$, which split the dimension with largest spread of the training data into two halves. Since sigmoid functions never reach 0 or 1, the described behavior is realized using saturating linear functions

$$p_i(\mathbf{x}) = \begin{cases} 0 & \text{if } x_{j_i} < s_i - \frac{o_i}{2} \\ \frac{x_{j_i} - s_i}{o_i} + \frac{1}{2} & \text{if } s_i - \frac{o_i}{2} \leq x_{j_i} \leq s_i + \frac{o_i}{2} \\ 1 & \text{if } s_i + \frac{o_i}{2} < x_{j_i}, \end{cases} \quad (7)$$

where j_i denotes the orthogonal dimension to the nominal dividing hyperplane, s_i is the position of the nominal dividing hyperplane, and o_i is the size of the overlapping region. The effect of these parameters on the active region of the models is depicted in Fig. 1. In order to determine the parameters for each conditional probability $p_i(\cdot)$, we compute the width vector \mathbf{w}_i , whose elements are defined as $w_{i,j} = (\max_{\mathbf{x} \in \mathbb{D}_i} x_j - \min_{\mathbf{x} \in \mathbb{D}_i} x_j)$. Based on this vector, we determine the division dimension $j_i = \arg \max_{j=1, \dots, d} w_{i,j}$, the position of the dividing hyperplane $s_i = \sum_{\mathbf{x} \in \mathbb{D}_i} x_{j_i} / \bar{N}$ and the size of the overlapping region as $o_i = \theta w_{i,j}$, where $\theta \in \mathbb{R}_+$ is the overlap ratio. A detailed evaluation of the effect of these definitions on the performance of the DLGP method is provided in Appendix B.

Due to the spatial separation of the models, the complexity of predictions significantly reduces. In fact, when the regions, in which local models are active, have similar extensions and the overlap ratio θ is chosen sufficiently small, it is straightforward to see that there exists a number $N_{\max}(\theta)$

such that the number of active models is bounded by 2^d (number of corners of a d -dimensional hypercube) for all $N \leq N_{\max}(\theta)$. Therefore, the efficiency of predictions can be improved by recursively following the paths towards leaf nodes, such that the marginal probabilities $\tilde{p}_j(\mathbf{x})$ of all descendants can be immediately set to 0 once a conditional probability $p_i(\mathbf{x}) = 0$ is encountered. Thereby, only 2^d marginal probabilities $\tilde{p}_j(\mathbf{x})$ must be computed, each of which requires multiplying $\mathcal{O}(\log(N))$ conditional probabilities in a branch of a balanced binary tree. Therefore, the complexity of predictions reduces to an $\mathcal{O}(2^d(\log(N) + \bar{N}))$ and $\mathcal{O}(2^d(\log(N) + \bar{N}^2))$ behavior of the mean and variance computations for $N \leq N_{\max}(\theta)$ in a balanced tree.

4 Numerical Evaluation

In order to demonstrate the computational efficiency and the prediction performance of DLGPs, we compare them to several state-of-the-art online regression approaches on real world, real-time learning data sets. In Section 4.1, we briefly introduce the used data sets as well as the comparison methods. The results of the numerical experiment are provided in Section 4.2.

4.1 Setup

For efficiency and performance comparison, we compare the following state-of-the-art real-time GP regression approaches and LWPR:

- our DLGP method with a fraction of the overlapping region $\theta = 0.05$ and a maximum number of $\bar{N} = 100$ points per local model
- our DLGP method with $\theta = 0.05$ and $\bar{N} = 500$
- local GPs [40] with a maximum of $\bar{N} = 500$ training samples per model, a threshold \bar{w} , such that approximately 30 local models are generated, and the insertion of training points based on the information gain criterion¹
- the SONIG algorithm [10], which is an online FITC approach, with inducing input point distance 4 and small training input noise variance of 10^{-6} , since this algorithm is designed for noisy training inputs²
- the deterministic training point conditional (DTC) approximation with the maximum error criterion for insertion and deletion of training data from the active set [8] combined with an straightforward adaptation of the sparse online GP algorithm [24]; the threshold for insertion is set to 25% of the standard deviation of the target values corresponding to a joint
- the incremental sparse spectrum GP (I-SSGP) approach [34], in which the covariance function of the GP is approximated using 200 sinusoidal random features
- the LWPR toolbox [14] with initial distance metrics $0.5\mathbf{I}$, initial learning rate of 0.5 and 0.3 as weight activation threshold³
- exact GP regression computed using blackbox matrix-matrix inference parallelized on GPUs [43] as a baseline for the prediction performance; the precision of the employed conjugate gradient algorithm is set to 0.01⁴

We compare these methods in two different scenarios for learning of the inverse dynamics of robotic manipulators, which is a common real-time learning problem. In the first scenario, we evaluate the performance on the SARCOS data set⁵, which consists of 44484 training points with $d = 21$ dimensional inputs and 7 dimensional targets corresponding to the joints of the robot, which are learned independently. A subset of 4449 samples of the training data is used as test set to analyze the capabilities of the real-time learning methods to represent nonlinear functions and monitor the learning progress. We use GPs with squared exponential kernels, and the hyperparameters are determined a priori based on log-likelihood maximization with the GPyTorch toolbox [44] using 100

¹we used code from <https://www.ias.informatik.tu-darmstadt.de/Miscellaneous/>

²we used code from <https://github.com/HildoBijl/SONIG/>

³we used code from <http://wcms.inf.ed.ac.uk/ipab/slmc/research/software-lwpr/>

⁴we used code from <https://github.com/cornellius-gp/gpytorch/>

⁵data available at <http://www.gaussianprocess.org/gpml/data/>

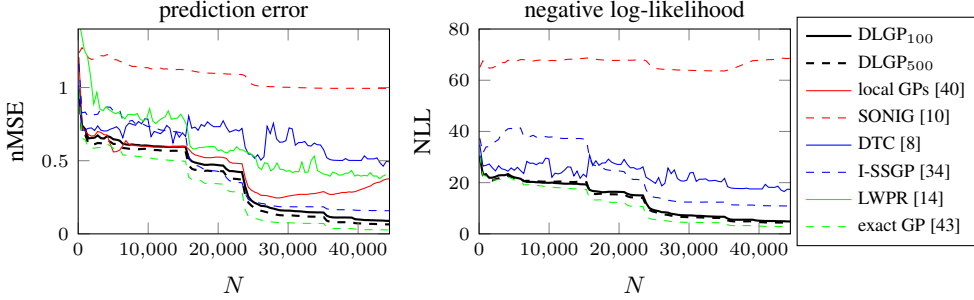


Figure 2: Left: The nMSE of the DLGPs is comparable to state-of-the-art online regression methods for small and medium numbers of training samples, but keeps decreasing when other methods effectively stop learning. Right: DLGPs provide high quality predictive distributions similar to exact GPs for joint 1 of the SARCOS data set, while this is an issue in existing approaches.

Table 1: Prediction performance (nMSE with NLL in brackets, where available) for the SARCOS data set after observation of all training samples with the results from exact GP regression as baseline from an off-line method; J_i denotes the i -th joint.

	DLGP ₁₀₀	DLGP ₅₀₀	local GPs	SONIG	DTC	I-SSGP	LWPR	exact GP
J_1	0.08(4.8)	0.07(4.3)	0.38	0.99(68.6)	0.49(17.4)	0.16(10.9)	0.39	0.03(2.8)
J_2	0.12(4.0)	0.10(3.7)	0.66	1.94(81.2)	0.87(17.6)	0.30(11.2)	0.25	0.04(2.5)
J_3	0.06(2.2)	0.05(2.1)	0.29	1.21(36.5)	0.52(6.0)	0.11(3.2)	0.16	0.02(1.9)
J_4	0.06(2.4)	0.03(2.2)	0.54	2.25(119.3)	0.36(7.3)	0.13(5.2)	0.26	0.01(1.8)
J_5	0.01(-1.0)	0.02(-1.0)	0.24	1.19(2.4)	0.85(11.0)	0.33(27.6)	0.17	0.007(-0.2)
J_6	0.01(-0.5)	0.01(0.0)	0.18	0.92(2.5)	0.51(0.1)	0.15(64.6)	0.4	0.008(0.2)
J_7	0.04(1.5)	0.03(1.5)	0.39	1.56(5.2)	0.32(1.8)	0.11(1.6)	0.17	0.01(1.6)

iterations of conjugate gradient optimization. After this initial hyperparameter optimization, we keep them constant, and we investigate the learning progress after adding new data points at 100 uniformly spaced numbers of training samples in the interval [100, 44484]. For each joint, we determine the normalized mean square error (nMSE) of the evaluation on the test data following the definition of [40]. Moreover, we determine the negative log-likelihood (NLL) averaged over the individual test predictions, whenever the learned model provides a predictive distribution (all except local GPs and LWPR). This allows to investigate the quality of the posterior variance for determining the model uncertainty. Finally, we measure the average update and prediction times, for which we only take the computations of the mean function (5) into account in order to allow a fair comparison between methods with and without predictive distributions.

In the second scenario, we focus on the more realistic real-time learning problem of iterating between updates with a single data point and predictions of the next target value as proposed in [34]. For this scenario, we employ the KUKA flask pushing data set⁶, which contains data of a KUKA robot arm pushing around flasks with different fill levels [45]. We follow the approach proposed in [34] and determine the hyperparameters based on 16940 measurements of experiments with a fill level of 300ml, while the methods are evaluated with a data set of 112761 samples of experiments with fill levels of 200ml and 400ml. Due to these different fill levels in the offline and online data, as well as changing fill levels in the online data, this data set presents a challenging real-time learning problem. Each training pair consists of a $d = 15$ dimensional input and 5 target values corresponding to joints of the robotic manipulator, which are learned independently with the different methods. The prediction performance is evaluated based on the nMSE, where the mean is taken over all predictions, and we analogously determine the average of the NLL to analyze the quality of the predictive distributions.

4.2 Results

The prediction error and negative log-likelihood development of the different online regression methods for joint 1 of the SARCOS data set are depicted in Fig. 2.⁷ As shown at the left hand-side for the regression error, both DLGPs outperform existing online regression methods regarding the

⁶data available at <https://robotics.com.de/ds/>

⁷Detailed simulation results for both scenarios and all joints can be found in Appendix C.

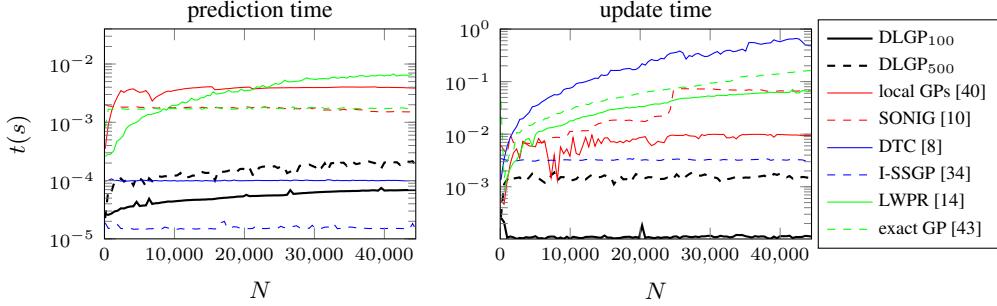


Figure 3: Left: The prediction time of DLGPs increases logarithmically on the SARCOS data set (joint 1), and remains smaller than for many existing methods. Right: The update time of DLGPs is almost constant due to a slow logarithmic growth, such that the DLGP method is significantly faster than all state-of-the-art methods.

regression error for large numbers of training samples, and exhibit at least comparable performance for small and medium training set sizes. Only the exact GP provides a better performance, since it is an offline learning method, and merely serves as baseline to demonstrate the high regression quality of the DLGP approach. Although the local GP approach [40] as well as the I-SSGP method [34] exhibit a learning behavior comparable to DLGPs at the beginning, only DLGPs are capable of learning from all the data, while other methods stop prematurely due to limited expressiveness. The NLL curves, which are depicted at the right hand-side of Fig. 2, exhibit a similar behavior: both DLGPs results are close to the exact GP, while the I-SSGP curve exhibits a far larger offset and the NLL of other methods is barely affected by additional data. These results generally repeat for the other joints, as summarized by Table 1, which displays the results after observation of all training samples. The excellent predictive distributions of DLGPs are especially remarkable, since many GP approximations are known to suffer from bad posterior variance estimates [46]. For joints 6 and 7, the NLL of the DLGPs is even lower than the corresponding values of the exact GP, which is a consequence of the localizing data set division, such that only training samples close to a test point are employed for prediction. However, when this improvement over exact GPs occurs, it has the unintuitive side effect that an increase in \bar{N} causes an almost negligible prediction performance deterioration.

Since small numbers \bar{N} are preferable due to lower computational complexity, this slight deterioration is not a critical disadvantage. The effect of different values for \bar{N} can be seen at the left-hand side of Fig. 3, which depicts the average computation time of predictions for the different methods. The higher value of \bar{N} slows down the prediction, but the prediction times of both DLGPs grow slowly and in fact exhibit a logarithmic dependency on the number of training samples N . Although other methods such as the online GP with DTC approximation [8] and the I-SSGP [34] have constant prediction times, DLGPs are only slightly slower and could be further sped up by reducing \bar{N} or reducing the overlap ratio θ . Moreover, both DLGPs significantly outperform the state-of-the-art method regarding the average update time, as illustrated at the right-hand side of Fig. 3. While other methods exhibit a linear growth in update time, it grows logarithmically for the DLGPs, which almost seems constant due to the small slope. Thereby, DLGPs achieve even lower update times than methods with constant update complexity such as I-SSGP, and allow predictions **and** updates at the high rates necessary for real-time learning.

When applying the methods to the real-time learning problem in our second scenario, similar results for the prediction errors and predictive distributions can be observed, as summarized in Table 2. However, the advantages of local training sets can be seen even more strongly since even the local GP approach exhibits better performance than many other approaches. Therefore, the DLGP with $\bar{N} = 100$ exhibits slightly better performance than our second DLGP with higher value of \bar{N} . Despite of this unintuitive behavior, both DLGPs outperform all other methods in terms of the nMSE and NLL. Therefore, DLGPs are particularly suited for real-time regression problems due to the high prediction accuracy, trustworthy predictive distributions as well as low update and prediction times.

5 Conclusion

This paper presents a novel online regression method, which bases on the division of local Gaussian process models. It allows to perform updates for new incoming data points and predictions with

Table 2: Prediction performance (nMSE and NLL in brackets) for the KUKA flask pushing data set after observation of all training samples; exact GP regression cannot be evaluated due to exceedingly high computation time; J_i denotes the i -th joint.

	DLGP ₁₀₀	DLGP ₅₀₀	local GPs	SONIG	DTC	I-SSGP	LWPR
J_1	0.04(-2.8)	0.04(-2.8)	0.08	0.81(-0.3)	0.82(28.3)	0.13(5.4)	0.34
J_2	0.06(-2.8)	0.06(-2.8)	0.09	0.84(-0.5)	0.95(19.0)	0.16(4.3)	0.50
J_3	0.09(-2.9)	0.11(-2.7)	0.31	0.87(-0.9)	0.89(23.8)	0.24(5.1)	0.53
J_4	0.04(-2.8)	0.04(-2.7)	0.13	0.73(0.2)	0.73(20.3)	0.12(11.1)	0.32
J_5	0.07(-2.8)	0.08(-2.7)	0.08	1.00(0.9)	0.98(14.6)	0.24(17.7)	0.69

logarithmic complexity in practice. Our numerical evaluation shows, that the accuracy is higher than for most existing methods and particularly shows advantages for large data sets. Moreover, the predictive distributions are more reliable and update times are significantly below the state of the art.

Broader Impact

The major positive outcome of the presented research lies in the development of an online applicable regression method for fast processes in sequential decision making problems. The proposed method neither provides direct benefits to anybody, nor does it put anybody at disadvantage. There is no immediate consequence of failure for online regression, and similarly, biases are not actively exploited.

References

- [1] O. Andersson, M. Wzorek, and P. Doherty, “Deep learning quadcopter control via risk-aware active learning,” in *Proceedings of the 31st AAAI Conference on Artificial Intelligence*, 2017, pp. 3812–3818.
- [2] D. Nguyen-Tuong and J. Peters, “Incremental sparsification for real-time online model learning,” *Journal of Machine Learning Research*, vol. 9, pp. 557–564, 2010.
- [3] S. Lee, H. Choi, and K. Min, “Reduction of Engine Emissions via a Real-Time Engine Combustion Control with an EGR Rate Estimation Model,” *International Journal of Automotive Technology*, vol. 18, no. 4, pp. 571–578, 2017.
- [4] M. Hafner, M. Schüler, O. Nelles, and R. Isermann, “Fast neural networks for diesel engine control design,” *Control Engineering Practice*, vol. 8, no. 11, pp. 1211–1221, 2000.
- [5] J. Kong, M. Pfeiffer, G. Schildbach, and F. Borrelli, “Kinematic and dynamic vehicle models for autonomous driving control design,” in *Proceedings of the IEEE Intelligent Vehicles Symposium*, 2015, pp. 1094–1099.
- [6] D. Nguyen-Tuong and J. Peters, “Model learning for robot control: A survey,” *Cognitive Processing*, vol. 12, no. 4, pp. 319–340, 2011.
- [7] C. E. Rasmussen and C. K. I. Williams, *Gaussian Processes for Machine Learning*. Cambridge, MA: The MIT Press, 2006.
- [8] J. Schreiter, D. Nguyen-Tuong, and M. Toussaint, “Efficient sparsification for Gaussian process regression,” *Neurocomputing*, vol. 192, no. May, pp. 29–37, 2016. [Online]. Available: <http://dx.doi.org/10.1016/j.neucom.2016.02.032>
- [9] M. F. Huber, “Recursive Gaussian process: On-line regression and learning,” *Pattern Recognition Letters*, vol. 45, no. 1, pp. 85–91, 2014.
- [10] H. Bijl, T. B. Schön, J.-W. van Wingerden, and M. Verhaegen, “System identification through online sparse Gaussian process regression with input noise,” *IFAC Journal of Systems and Control*, vol. 2, pp. 1–11, 2017.
- [11] J. Umlauft and S. Hirche, “Feedback Linearization based on Gaussian Processes with event-triggered Online Learning,” *IEEE Transactions on Automatic Control*, 2020.

- [12] T. Koller, F. Berkenkamp, M. Turchetta, and A. Krause, “Learning-based Model Predictive Control for Safe Exploration,” in *Proceedings of the IEEE Conference on Decision and Control*, 2018, pp. 6059–6066.
- [13] J. Ma, J. Theiler, and S. Perkins, “Accurate On-line Support Vector Regression,” *Neural Computation*, vol. 15, no. 11, pp. 2683–2703, 2003.
- [14] S. Vijayakumar and S. Schaal, “Locally Weighted Projection Regression: An O(n) Algorithm for Incremental Real Time Learning in High Dimensional Space,” *Proceedings of the Seventeenth International Conference on Machine Learning*, vol. 1086, pp. 1079–1086, 2000.
- [15] S. Vijayakumar, A. D’Souza, and S. Schaal, “Incremental online learning in high dimensions,” *Neural Computation*, vol. 17, no. 12, pp. 2602–2634, 2005.
- [16] S. Klanke, S. Vijayakumar, and S. Schaal, “A library for locally weighted projection regression,” *Journal of Machine Learning Research*, vol. 9, pp. 623–626, 2008.
- [17] G. Fagogenis, C. Bergeles, and P. E. Dupont, “Adaptive nonparametric kinematic modeling of concentric tube robots,” in *Proceedings of the IEEE International Conference on Intelligent Robots and Systems*. IEEE, 2016, pp. 4324–4329.
- [18] R. Grandia, D. Pardo, and J. Buchli, “Contact Invariant Model Learning for Legged Robot Locomotion,” *IEEE Robotics and Automation Letters*, vol. 3, no. 3, pp. 2291–2298, 2018.
- [19] T. Gao, S. Yin, H. Gao, X. Yang, J. Qiu, and O. Kaynak, “A Locally Weighted Project Regression Approach-Aided Nonlinear Constrained Tracking Control,” *IEEE Transactions on Neural Networks and Learning Systems*, vol. 29, no. 12, pp. 5870–5879, 2018.
- [20] F. Meier, P. Hennig, and S. Schaal, “Incremental local Gaussian regression,” in *Advances in Neural Information Processing Systems*, 2014, pp. 972–980.
- [21] ——, “Efficient Bayesian local model learning for control,” *Proceedings of the 2014 IEEE/RSJ International Conference on Intelligent Robots and Systems*, pp. 2244–2249, 2014.
- [22] J. Luts, T. Broderick, and M. P. Wand, “Real-Time Semiparametric Regression,” *Journal of Computational and Graphical Statistics*, vol. 23, no. 3, pp. 589–615, 2014.
- [23] E. Snelson and Z. Ghahramani, “Local and global sparse Gaussian process approximations,” *Journal of Machine Learning Research*, vol. 2, pp. 524–531, 2007.
- [24] L. Csató and M. Opper, “Sparse on-line gaussian processes,” *Neural Computation*, vol. 14, no. 3, pp. 641–668, 2002.
- [25] A. Koppel, “Consistent Online Gaussian Process Regression Without the Sample Complexity Bottleneck,” in *Proceedings of the American Control Conference*, 2019, pp. 3512–3518.
- [26] T. Le, K. Nguyen, V. Nguyen, T. D. Nguyen, and D. Phung, “GoGP: Fast online regression with Gaussian processes,” *Proceedings of the IEEE International Conference on Data Mining*, vol. 2017-Novem, pp. 257–266, 2017.
- [27] A. Ranganathan and M.-h. Yang, “Online Sparse Matrix Gaussian Process Regression and Vision Applications,” in *Proceedings of the European Conference on Computer Vision*, 2008, pp. 468–482.
- [28] A. Ranganathan, M. H. Yang, and J. Ho, “Online sparse gaussian process regression and its applications,” *IEEE Transactions on Image Processing*, vol. 20, no. 2, pp. 391–404, 2011.
- [29] T. D. Bui, C. V. Nguyen, and R. E. Turner, “Streaming sparse Gaussian process approximations,” in *Advances in Neural Information Processing Systems*, 2017, pp. 3300–3308.
- [30] C. A. Cheng and B. Boots, “Incremental variational sparse Gaussian process regression,” in *Advances in Neural Information Processing Systems*, 2016, pp. 4410–4418.

- [31] J. Harrison, A. Sharma, and M. Pavone, “Meta-Learning Priors for Efficient Online Bayesian Regression,” in *Proceedings of the Workshop on the Algorithmic Foundations of Robotics*, 2018. [Online]. Available: <http://arxiv.org/abs/1807.08912>
- [32] R. Camoriano, S. Traversaro, L. Rosasco, G. Metta, and F. Nori, “Incremental semiparametric inverse dynamics learning,” in *Proceedings of the IEEE International Conference on Robotics and Automation*, 2016, pp. 544–550.
- [33] A. Rahimi and B. Recht, “Random features for large-scale kernel machines,” in *Advances in Neural Information Processing Systems*, 2008, pp. 1–8.
- [34] A. Gijsberts and G. Metta, “Real-time model learning using Incremental Sparse Spectrum Gaussian Process Regression,” *Neural Networks*, vol. 41, pp. 59–69, 2013.
- [35] Y. Gal and R. Turner, “Improving the Gaussian process sparse spectrum approximation by representing uncertainty in frequency inputs,” in *Proceedings of the 32nd International Conference on Machine Learning*, 2015, pp. 655–664.
- [36] H. Liu, Y.-S. Ong, X. Shen, and J. Cai, “When Gaussian Process Meets Big Data: A Review of Scalable GPs,” *IEEE Transactions on Neural Networks and Learning Systems*, pp. 1–20, 2020. [Online]. Available: <http://arxiv.org/abs/1807.01065>
- [37] M. van der Wilk, “Sparse Gaussian Process Approximations and Applications,” Ph.D. dissertation, University of Cambridge, 2018. [Online]. Available: <https://markvdw.github.io/vanderwilk-thesis.pdf>
- [38] D. Nguyen-Tuong, M. Seeger, and J. Peters, “Local Gaussian Process Regression for Real Time Online Model Learning and Control,” in *Advances in neural information processing systems*, 2009, pp. 1193–1200.
- [39] ——, “Computed Torque Control with Nonparametric Regression Models,” *Proceedings of the American Control Conference*, pp. 212–217, 2008.
- [40] ——, “Model learning with local Gaussian process regression,” *Advanced Robotics*, vol. 23, no. 15, pp. 2015–2034, 2009.
- [41] H. Xiao and C. Eckert, “Lazy Gaussian process committee for real-time online regression,” *Proceedings of the 27th AAAI Conference on Artificial Intelligence, AAAI 2013*, pp. 969–976, 2013.
- [42] F. Meier and S. Schaal, “Drifting Gaussian processes with varying neighborhood sizes for online model learning,” in *Proceedings of the IEEE International Conference on Robotics and Automation*. IEEE, 2016, pp. 264–269.
- [43] K. A. Wang, G. Pleiss, J. R. Gardner, S. Tyree, K. Q. Weinberger, and A. G. Wilson, “Exact Gaussian Processes on a Million Data Points,” in *Advances in Neural Information Processing Systems*, 2019, pp. 14 622–14 632.
- [44] J. R. Gardner, G. Pleiss, D. Bindel, K. Q. Weinberger, and A. G. Wilson, “Gpytorch: Black-box matrix-matrix Gaussian process inference with GPU acceleration,” in *Advances in Neural Information Processing Systems*, 2018, pp. 7576–7586.
- [45] E. Rueckert, M. Nakatenus, S. Tosatto, and J. Peters, “Learning inverse dynamics models in O(n) time with LSTM networks,” *Proceedings of the IEEE-RAS International Conference on Humanoid Robots*, pp. 811–816, 2017.
- [46] J. Quiñonero-candela, C. E. Rasmussen, and R. Herbrich, “A unifying view of sparse approximate Gaussian process regression,” *Journal of Machine Learning Research*, vol. 6, pp. 1935–1959, 2005.

A Hardware and Software used in the Simulations

All simulations were performed on a computer with an Intel(R) Core(TM) i9-9900X CPU and 128GB RAM. The GPU computations of exact GP regression were performed on two GeForce RTX 2080 Ti and one NVIDIA TITAN V GPUs. DLGPs, local GPs, SONIG, sparse GPs with DTC approximation and incremental sparse spectrum GPs were implemented using MATLAB R2019a, while for exact GPs a Python implementation was employed and LWPR is based on a C++ implementation.

B Further Information on the DLGP algorithm

This section provides details about the available parameters, the chosen values in the simulations and their influence on the performance of DLGP. In general and if not stated differently, the default parameters for a DLGP run are set to $\theta = 0.05$ for the fraction of the overlapping region and $\bar{N} = 100$ for the maximum number of points per local model. The nominal dividing hyperplane is positioned using the mean of the contained data points.

In the following, each data set for evaluating the impact of a parameter is generated by performing 100 Monte Carlo simulations in order to eliminate probabilistic effects of the random data assignment. Each figure depicts the mean (full lines) and standard deviation (shaded areas) of the Monte-Carlo simulations. The simulation scenario here is the same as the first one described in Section 4.1. While the data set is the same, the computation times are measured based on the mean and variance predictions, and thus, show increased values compared to the main article.

B.1 Position of the nominal dividing hyperplane

As described in Section 3.1, the position of the dividing hyperplane influences the data partitioning and has to be chosen such that the two resulting leaf nodes contain an approximately equal amount of points in order to achieve a balanced binary tree. Hence, natural ways of calculating s_i are

$$s_i = \text{med}_{\mathbf{x} \in \mathbb{D}_i}(x_{j_i}) \quad \forall x_{j_i} \in \mathbb{D} \quad (8)$$

$$s_i = \frac{1}{N} \sum_{\mathbf{x} \in \mathbb{D}_i} x_{j_i} \quad (9)$$

$$s_i = \frac{1}{2} \left(\max_{\mathbf{x} \in \mathbb{D}_i} x_{j_i} - \min_{\mathbf{x} \in \mathbb{D}_i} x_{j_i} \right), \quad (10)$$

where (8) and (9) use the median and mean, respectively, of all $\mathbf{x} \in \mathbb{D}_i$ in the j_i -th dimension, and (10) is based on half the distance between minimum and maximum of the data points. In the main article, the calculations and derivations use the strategy based on the mean value from (9).

Figure 4 provides a comparison of these three methods using the overall update and prediction times, normalized mean squared prediction error, average negative log-likelihood (NLL), number of tree divisions and the ratio O_D . This ratio is defined as the percentage of points, which lie in the overlapping region during all model divisions. It can be observed that no method significantly drops off in any of the provided measures. In contrast, the update time, prediction error and negative log-likelihood only differ in single-digit percentage ranges. However, there is a more substantial effect on the prediction time as the results obtained with (10) yield a 31% smaller time than the method from (8) while the number of divisions indicates a reverse behavior. The ratio O_D hereby allows a more indirect insight. While more points in the overlapping region theoretically lead to smoother functions in that region, less points entail less computational complexity and lower prediction times. This effect can be seen when comparing the ratio O_D with the prediction times in Figure 4 as they show a related behavior. Meanwhile, the number of divisions only has effects on the updating part of the GP and leaves the predictions unchanged.

Additionally, the plots in Figure 5 show the dependency on the training set size of the same simulation for prediction error, NLL, average update and prediction times, where especially for the accuracy measured by error, no significant difference is visible. However, the NLL of the median and minmax approach exhibit higher values than the mean division method, in particular at low num-

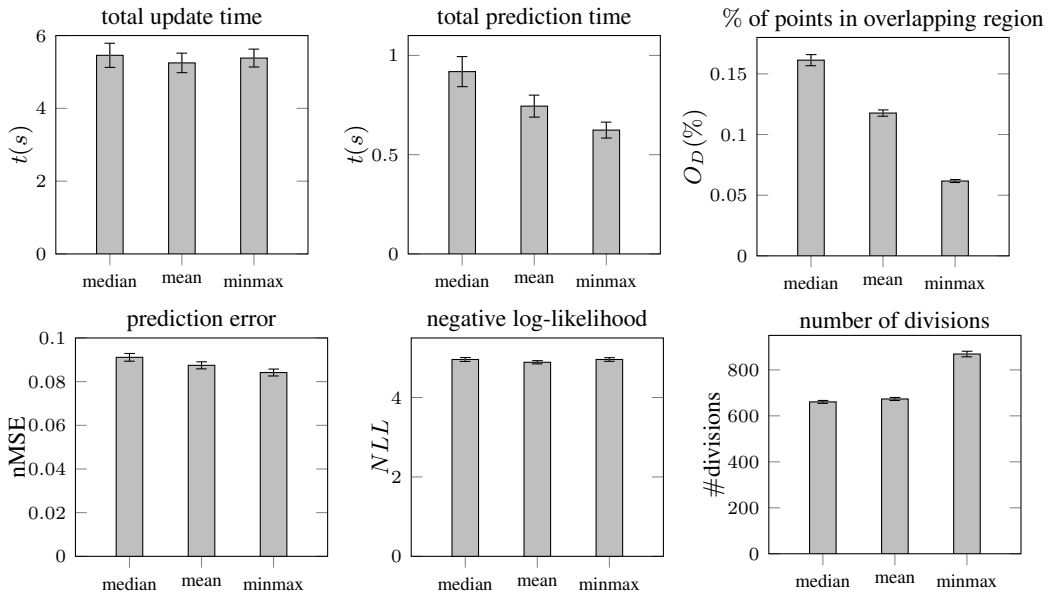


Figure 4: Comparison of strategies to obtain position of dividing hyperplane s_i , where the methods are mean, median and half distance between min and max (minmax).

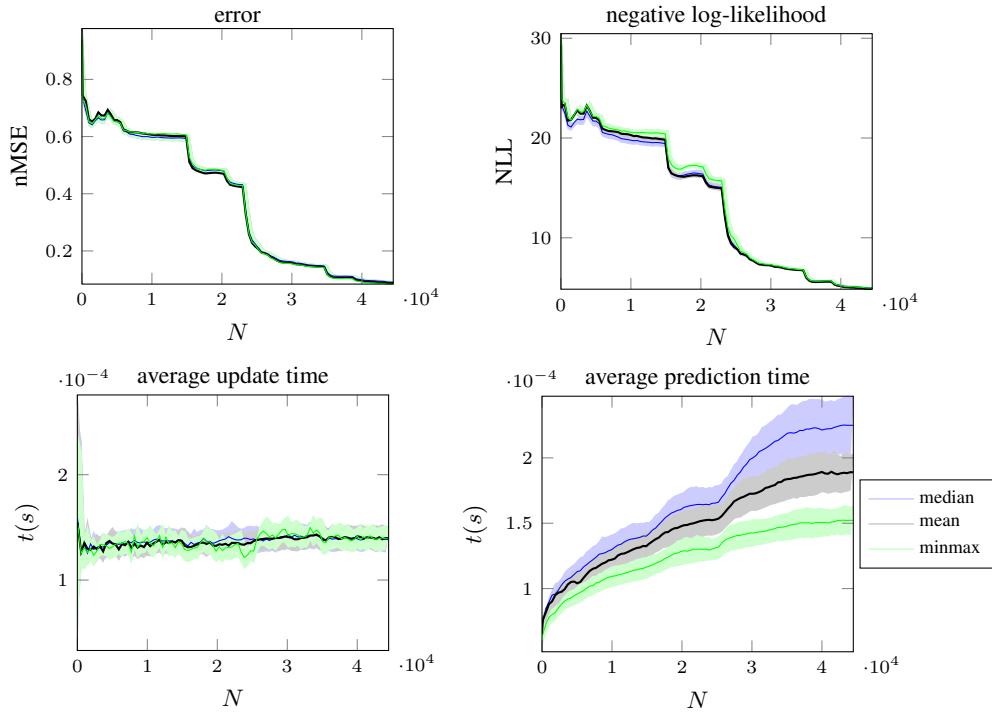


Figure 5: Prediction error, NLL, update and prediction time for joint 1 through the learning process obtained with different methods for choosing s_i .

bers of training samples. While the average update time evolves as discussed above independently of the amount of training data, the average prediction time is subject to few outliers in the median and distance based methods, with the mean being the smoothest approach.

In summary, the simulation results in Figures 4 and 5 allow to conclude that the performance cannot be influenced substantially by choosing a different dividing method, resulting in a robust interface for potential use-cases. However, it still provides room for tuning the performance in a certain domain if required by the application scenario. If a trade-off between all measures is required, using the mean (9) suggests the best result in this particular setup.

B.2 Overlapping factor

The overlapping factor θ allows to adjust the smoothness of the transition between two neighboring child sets in the binary tree. In general, a greater overlapping region is achieved by a larger θ , which yields a smoother model with the drawback of increased computational complexity of predictions.

Figure 6 depicts the influence of the overlapping factor on the same performance measures as in Section B.1. It is evident that θ has no effect on the update time, since the size of the overlapping region has no direct impact on the computational complexity of updates. Additionally, the almost linear dependency between the ratio O_D of points in the overlapping region and θ can be directly deduced. The higher the overlapping factor, the greater is the overlapping region with more points in it. The prediction performance in terms of computation times, error and NLL is affected strongly. The complexity analysis from Section 3.2 emerges especially for the total prediction time. With increasing θ , the predictions evolve from logarithmic to linear complexity since larger overlapping regions lead to more active local models such that more local predictions have to be calculated. As one can see in the NLL and error plots, the accuracy declines with an increasing θ . One reason for this lies in the constant number of samples N and the increasing number of divisions which leads to many local models with only a few data points. This suggests that the data assignment does not yield a tree with equally distributed points and a worsening accuracy in general.

Accordingly, Figure 7 shows these results depending on the number of training samples for joint 1. The NLL for $\theta = 0.3$ starts at a smaller value, but lower values of θ approach a similar performance with increasing N . In contrast, the errors start on a similar level, but the differences between the different values of θ increase. Finally, looking at the learning process in Figure 7 consolidates the findings regarding the computation times. For example, the choice of θ does not influence the average update time. For the average prediction time, once again the complexity discussion from the main article becomes clearly visible. Choosing a sufficiently small θ such that $N < N_{\max}(\theta)$ leads to a logarithmic complexity compared to a linear behavior for too large θ . Therefore, choosing reasonable parameters can drastically improve the performance by eliminating the linear computational complexity.

To summarize, the overlapping factor θ can have a great impact on the performance of predicting new incoming data. If θ is chosen sufficiently small, one can achieve logarithmic computational complexity for calculating mean and variance prediction, while also resulting in a good regression performance.

B.3 Data limit

The parameter for the data limit \bar{N} determines the amount of data samples per local model at which the division into two sub-models is performed. Going for a too high value of \bar{N} results in local models requiring a high computational effort while a too small value leads to a large number of local numbers typically causing a decreased regression performance.

For outlining the effects of \bar{N} on the learning process, the impact on prediction error, NLL, average update and prediction times, the ratio O_D and the number of divisions is evaluated first as depicted in Figure 8. It indicates that the update time is bounded by $\mathcal{O}(\log(N) + \bar{N}^3)$ as discussed in Section 3.1. Note that N is constant in this setting. Therefore, for high values of \bar{N} , the number of local models is becoming small such that the normally cubic growth is counterbalanced in part. The fact that increasing the data limit leads to fewer local models can be observed in the number of divisions, which is almost reciprocal to \bar{N} . This effect also influences the average prediction time, which initially grows quadratically in \bar{N} causing a quickly growing total prediction time. In contrast

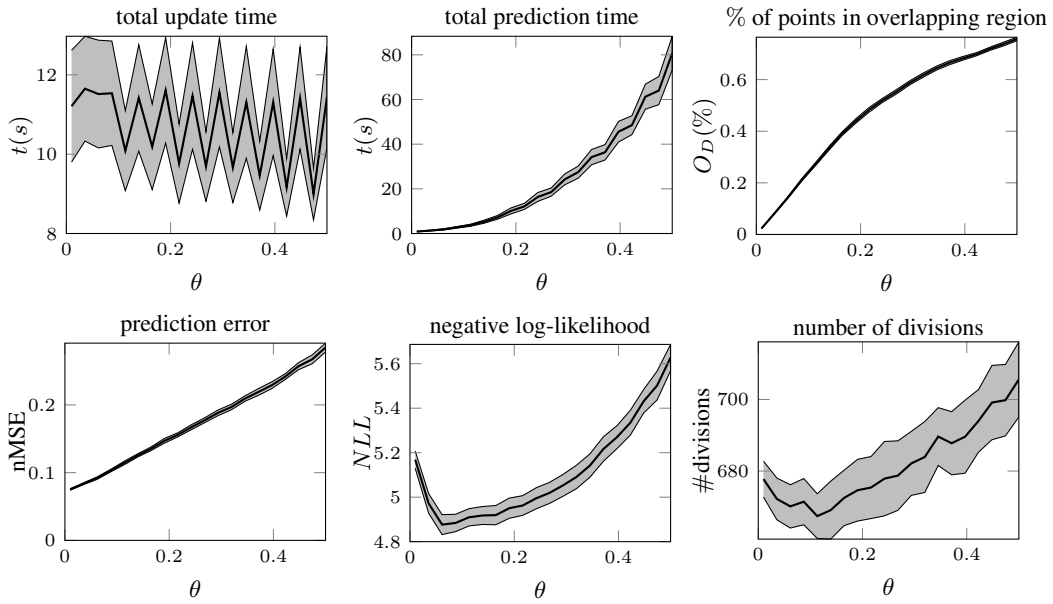


Figure 6: Influence of varying overlapping factor θ on the update and prediction time, prediction error, NLL, points in overlapping region and number of divisions.

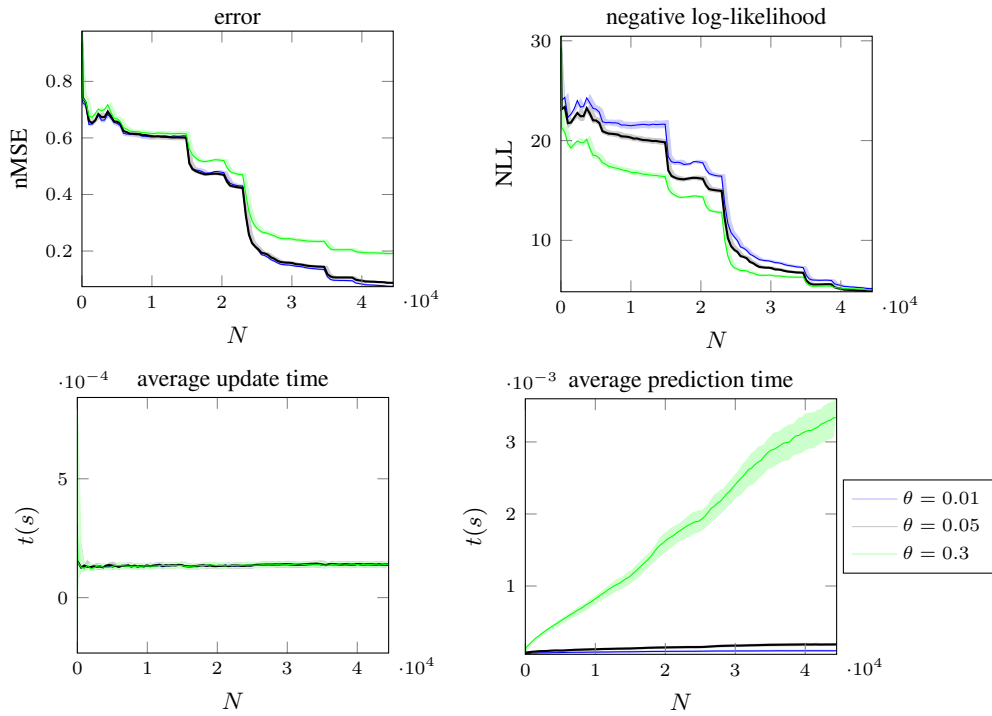


Figure 7: Prediction error, NLL, update and prediction time for joint 1 through the learning process obtained with different values for the overlapping factor θ .

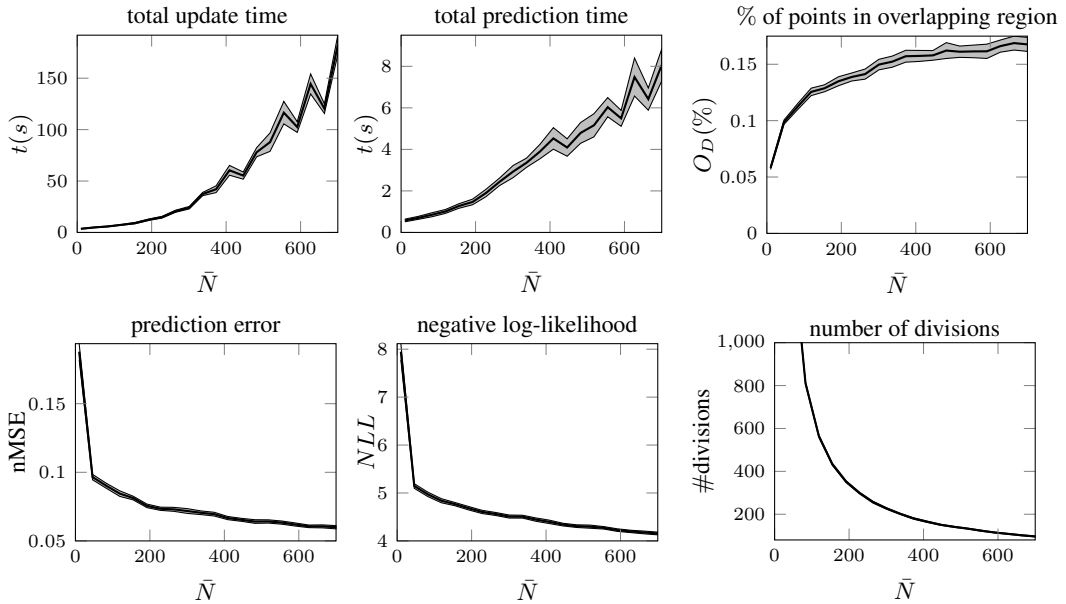


Figure 8: Influence of the data point limit \bar{N} on key performance measures.

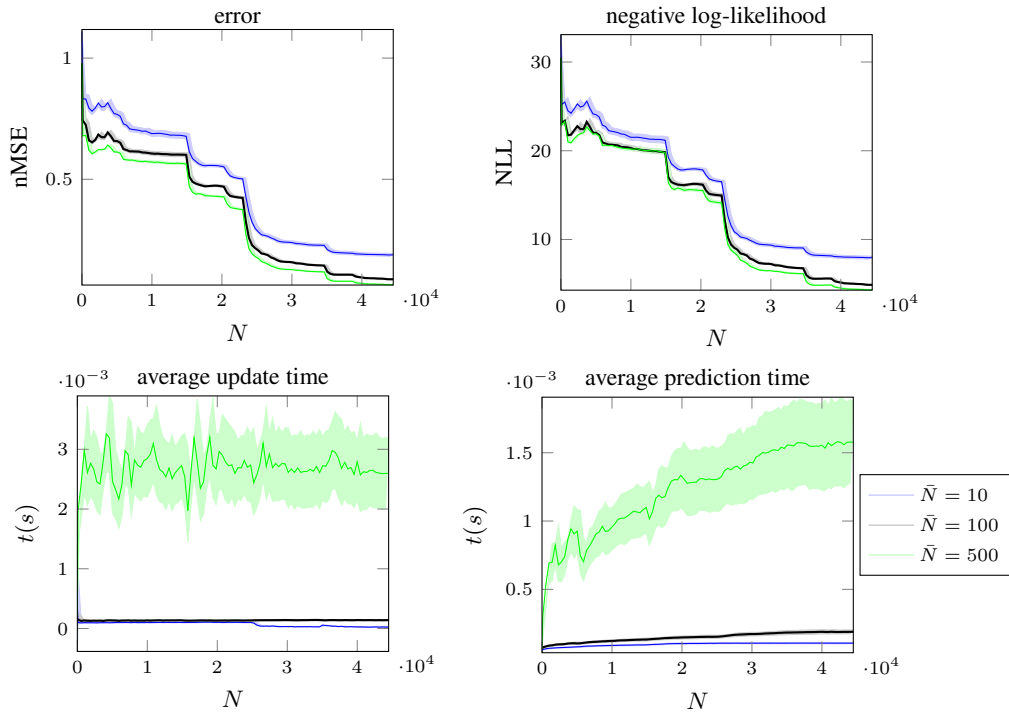


Figure 9: Prediction error, NLL, update and prediction time for joint 1 through the learning process obtained with different values of \bar{N} .

to the negative effect on the computation times, high values of \bar{N} are generally beneficial for the regression error and the quality of the predictive distributions. In fact, one can see the effect of a too small value of \bar{N} : If there are many local models, the amount of data points per model is too small, such that no meaningful local model can be learned. Therefore, a sufficiently high value of \bar{N} is necessary to learn useful local models.

Additionally, Figure 9 depicts the learning process for joint 1. One can clearly see the implications of too small and too high data limits \bar{N} . First, $\bar{N} = 10$ leads to a significantly worse accuracy as the error and NLL are constantly higher than for the remaining two simulations with higher values of \bar{N} . However, the timing behavior is better in accordance with the findings in Figure 8. In contrast, while a much higher $\bar{N} = 500$ shows a good regression performance, the increased computational effort also increases the average update and prediction times by an order of magnitude. For $\bar{N} = 100$, one can leverage the advantages and avoid the drawbacks of both too low and too high \bar{N} to some extent. Both, the accuracy in the error and NLL as well as the average update and prediction times remain in a similar range as the better performing parameter. Therefore, it stands to reason that \bar{N} is a good choice for a trade-off between good regression performance and reasonable computational effort.

C Additional Simulation Results

This section provides the detailed results corresponding to both scenarios outlined in Section 4.1. For each joint, the update times, prediction times, normalized mean squared error and average log-likelihood are depicted. While prediction times for the SARCOS data set are determined using mean predictions only, both mean and variance predictions are computed, when measuring the prediction time for the KUKA flask pushing data set.

C.1 SARCOS Data Set

Figures 10-13 depict the simulation results for the first scenario, which is evaluated on the SARCOS data set. The prediction error of the DLGPs, as illustrated in Fig. 10 exhibits the same behavior for all joints: it is almost parallel to the prediction error curve of exact GPs. Furthermore, the DLGPs outperform the other real-time learning approaches on all joints. While some other methods also show good regression performance, their variance predictions can be highly unreliable, as shown in Fig. 11. For some methods, the NLL is temporarily increasing despite of growing numbers of training samples, while the NLL is continuously decreasing for DLGPs. In fact, the NLL of the DLGPs is barely higher than for exact GPs, which underlines the high quality of the predictive distributions of DLGPs. In addition to the advantages regarding the predictive distributions, DLGPs also strongly benefit from low average update times, which allow real-time learning, as shown in Fig. 12. For all joints, the update time of DLGPs with $\bar{N} = 100$ is typically more than 10 times faster than for state-of-the-art methods. Moreover, the prediction time of the DLGPs, as illustrated in Fig. 13, exhibits a similar magnitude as the prediction time. Due to the slow growth of the prediction time, DLGPs allow similar prediction rates as many existing methods, while additionally updating the model with the same frequency.

C.2 KUKA Flask Pushing Data Set

Due to the different scenario, in which the KUKA flask pushing data set is learned, the performance measures are slightly adjusted. The prediction error is investigated using the online nMSE as defined in [34], which corresponds to the cumulative average normalized mean squared error. Analogously, we define the average online negative log-likelihood as the cumulative average NLL. In order to avoid overly noisy computation time estimates arising from single predictions or updates, we apply a moving average filter with filter width 1,000 to the update and prediction times.

The simulation results of the second scenario on the KUKA flask pushing data set are depicted in Figs. 14-17. As clearly shown in Fig. 14, the prediction error of almost all methods suffers from a sudden increase after approximately 23,000 data points of the online data for almost all joints, which is due to an outlier both in the targets and inputs. Local GPs do not exhibit a step in the error curves, but the error starts to increase after the outlier. While DLGPs suffer from a step similar to I-SSGPs, they convince through a continuously improving error afterwards, while the prediction error of other methods remains constant or even increases for some joints. The reason for this

behavior is the division of local models, which ensures that an outlier can have an effect only in its neighborhood, which becomes smaller when more data becomes available. As this effect is stronger, when each local model contains fewer samples, it is clear that the DLGP with $\bar{N} = 100$ outperforms the DLGP with $\bar{N} = 500$. The outlier has an even stronger impact on the predictive distributions of most models, as indicated in Fig. 15. While DLGPs exhibit a continuously low average NLL with merely a small increase after 23,000 samples, methods such as I-SSGP or sparse online GPs with DTC approximation exhibit rapid increases in the average NLL. Therefore, one of the main strengths of DLGPs is their capability of providing reliable predictive distributions, while other methods are often over-confident. In addition, the slow logarithmic growth of the update complexity of DLGPs leads to an almost constant average update time for large numbers of training samples, which is lower than for most other methods. This is depicted in Fig. 16, where it should be noted that all figures in the second scenario only display the results on the online data. Hence, $N = 0$ in the figures corresponds to models, which have already been trained using 16,940 offline samples. Although SONIG is faster than the DLGPs, this is caused by a very small active set, which in turn results in poor learning performance. Therefore, the DLGP with $\bar{N} = 100$ samples is the only method providing fast update rates and good learning performance. Finally, the prediction times of DLGPs are comparable to many state-of-the-art approaches, as shown in Fig. 17. The logarithmic growth in complexity merely causes a prediction time increase by a factor of approximately 2, when adding more than 10^5 training samples. Although other methods are faster in prediction, the prediction times of DLGPs could be easily reduced through a decrease of θ and \bar{N} as discussed in Appendix B. Thereby, it is straightforward to tune both parameters under consideration of constraints on the prediction and update times.

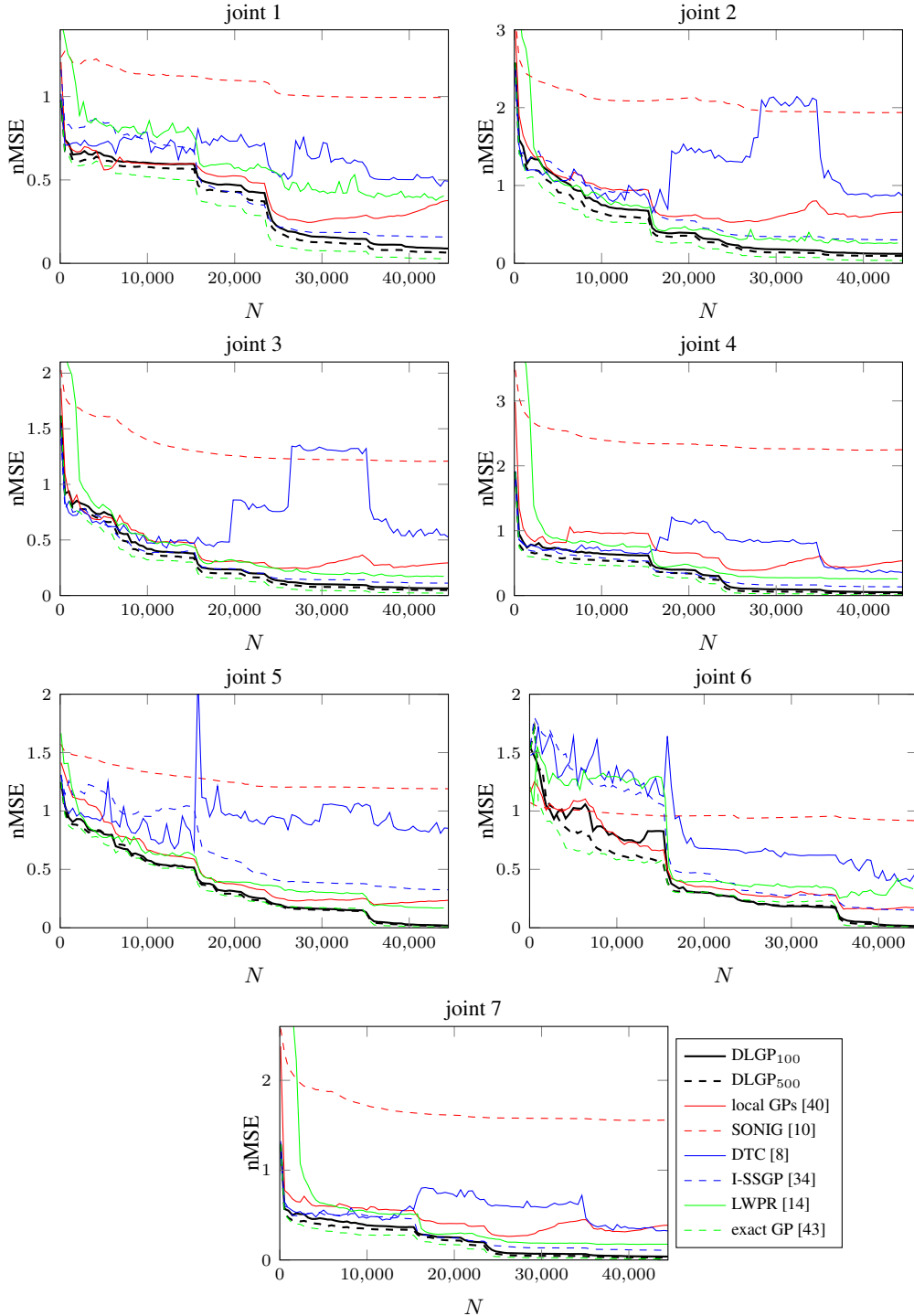


Figure 10: Normalized mean squared errors depending on the number of training samples N for all joints of the SARCOS data set: DLGPs consistently outperform other online regression methods and exhibit identical learning behavior as exact GP regression.

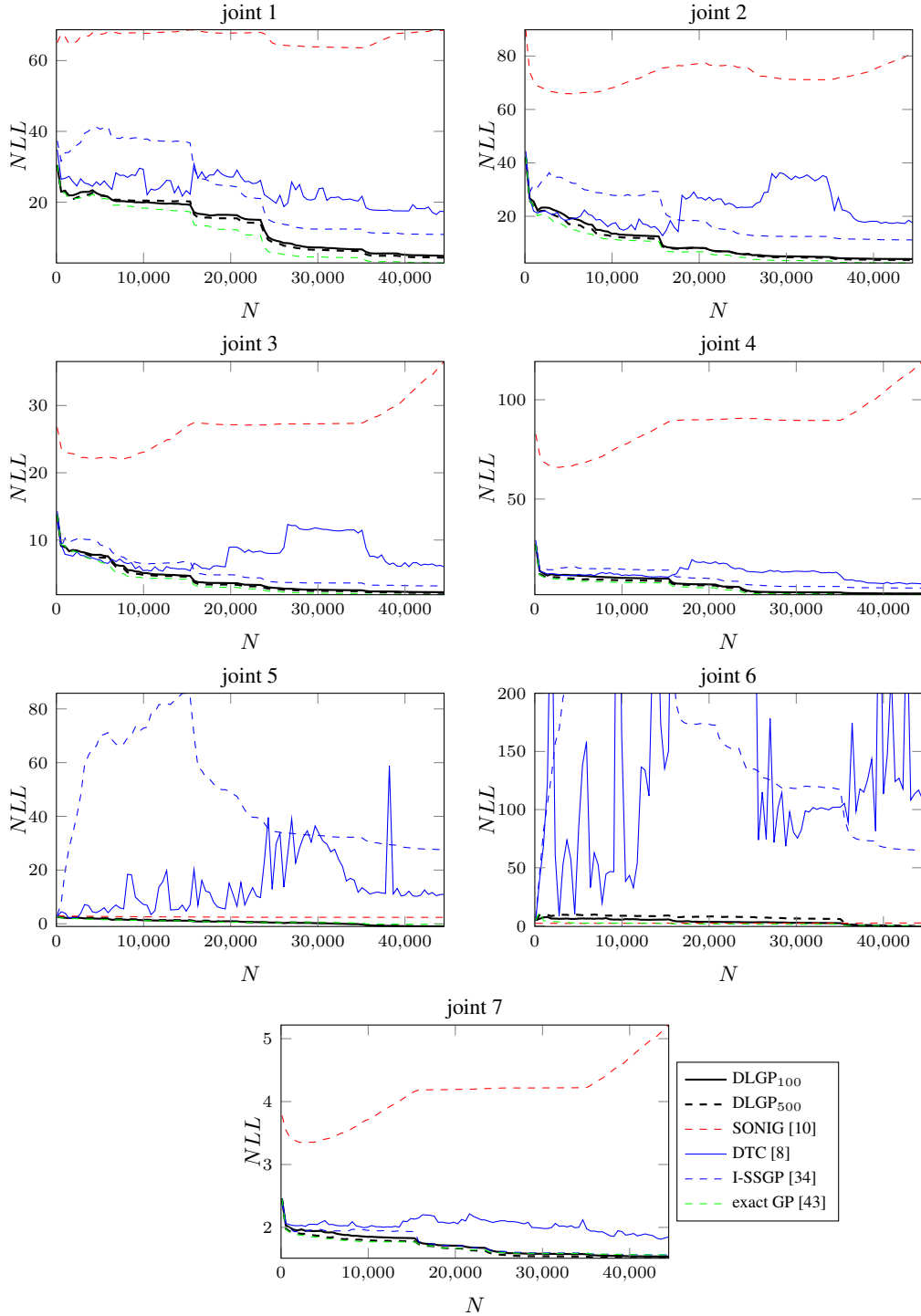


Figure 11: Average negative log-likelihood depending on the number of training samples N for all joints of the SARCOS data set: while some methods achieve reliable predictive distributions only for certain joints, DLGPs exhibit a performance similar to exact GPs.

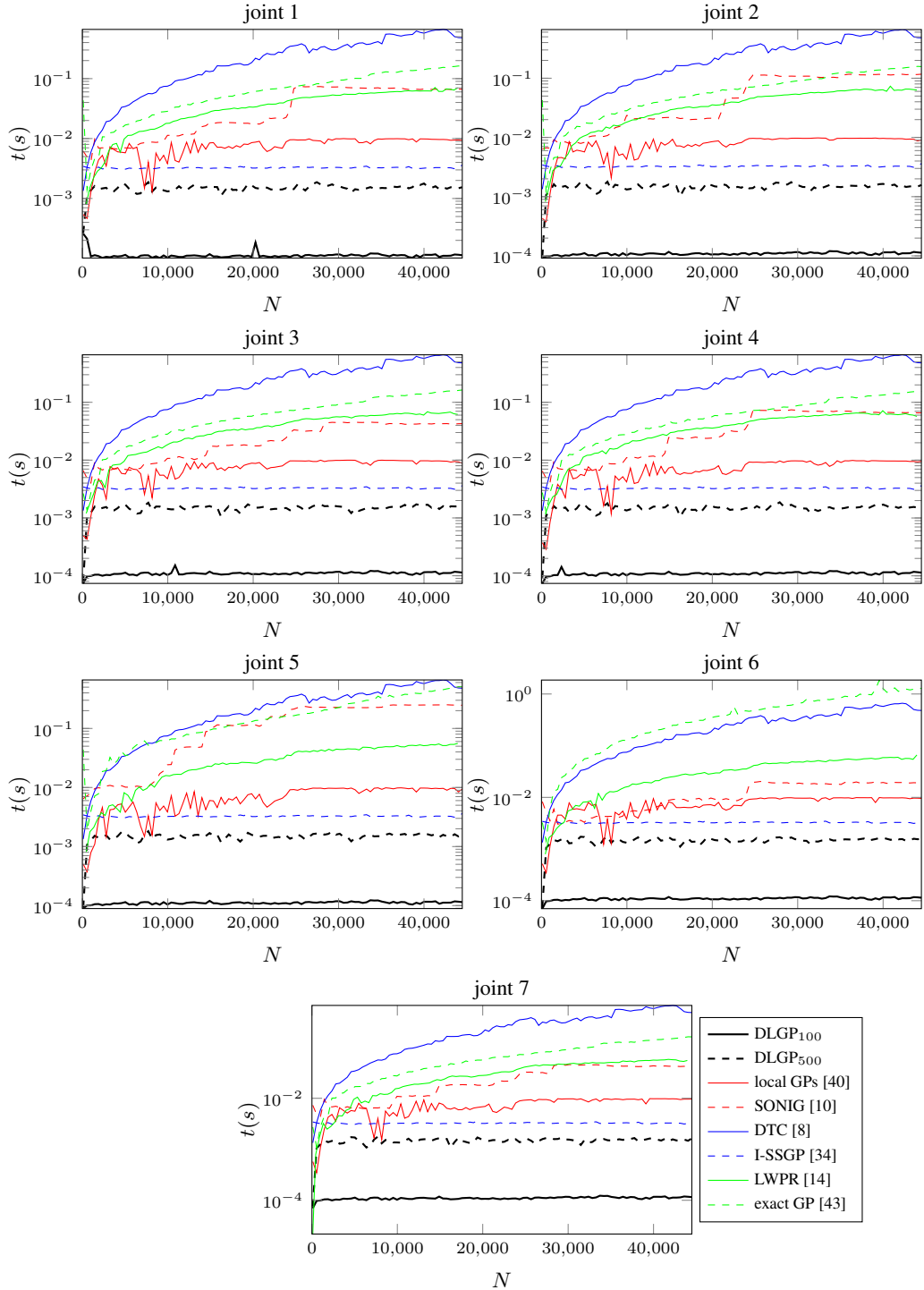


Figure 12: Average time necessary to update a model depending on the number of training samples N for all joints of the SARCOS data set: in contrast to other methods, the computational complexity of DLGPs does not depend on the training targets, resulting in almost identical curves for the different joints.

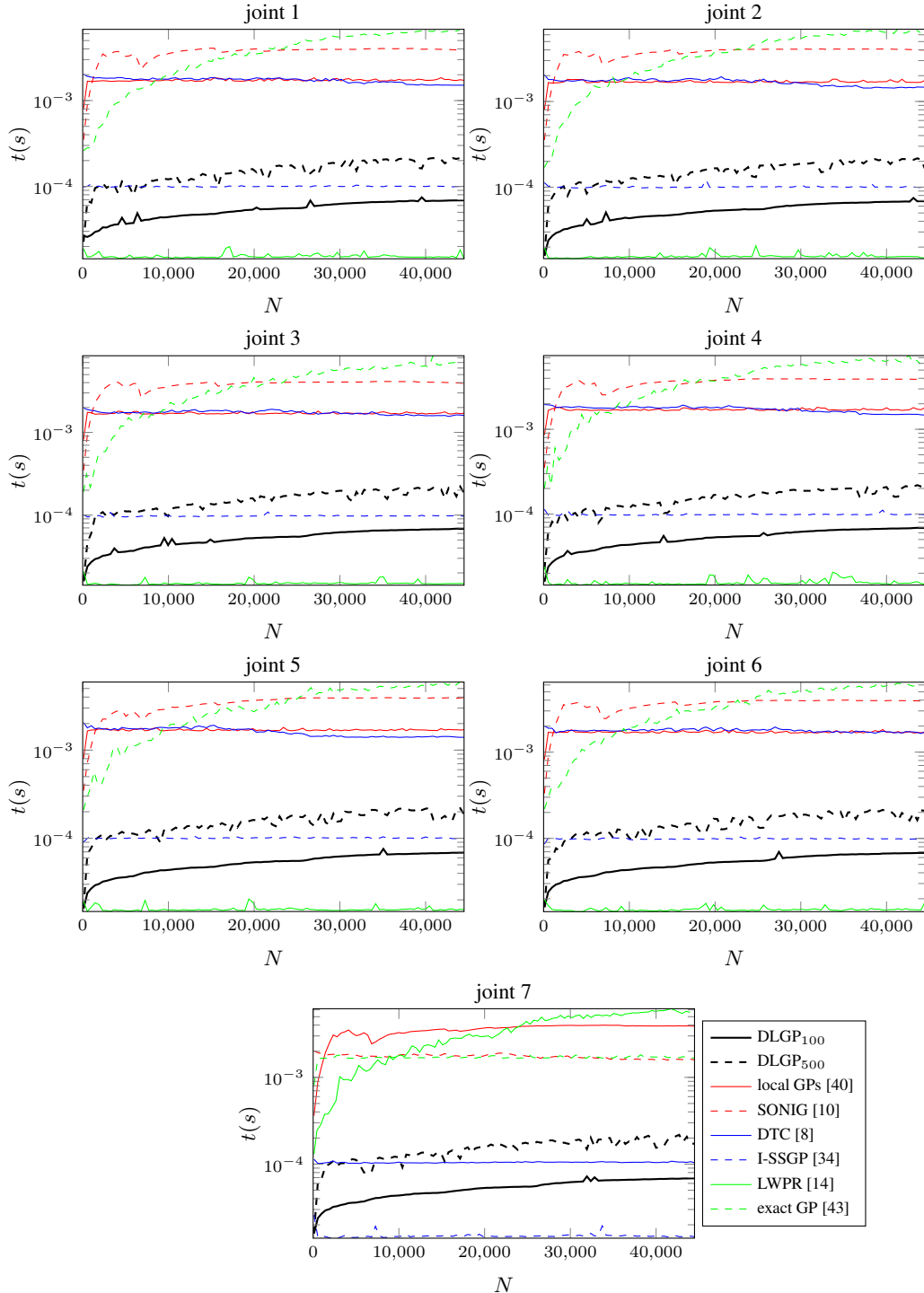


Figure 13: Average time necessary to compute a prediction depending on the number of training samples N for all joints of the SARCOS data set: DLGPs are faster than most other methods and exhibit only a slow, logarithmic increase in computation time.

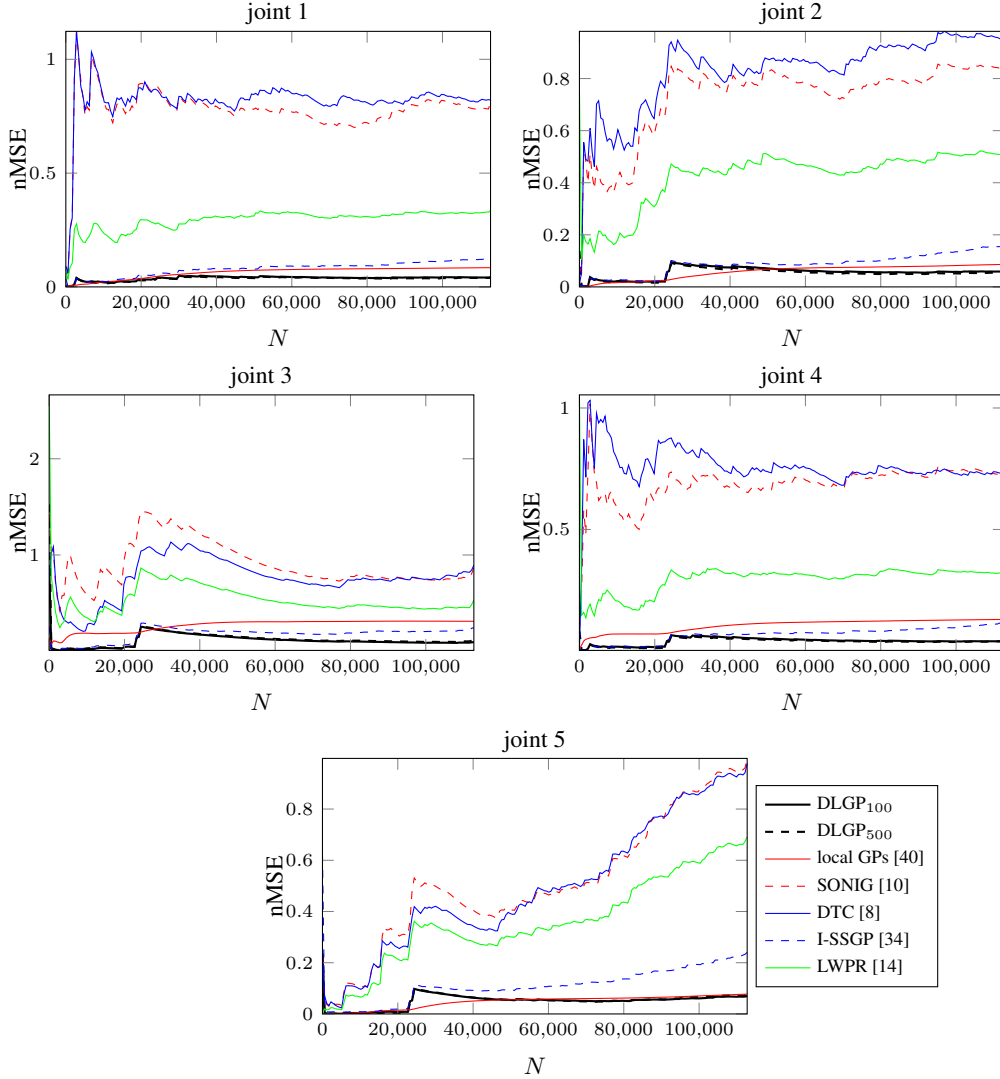


Figure 14: Online normalized mean squared errors for all joints of the KUKA flask pushing data set: DLGPs exhibit low regression errors and are capable of recovering from sudden environmental changes causing brief steps in the error.

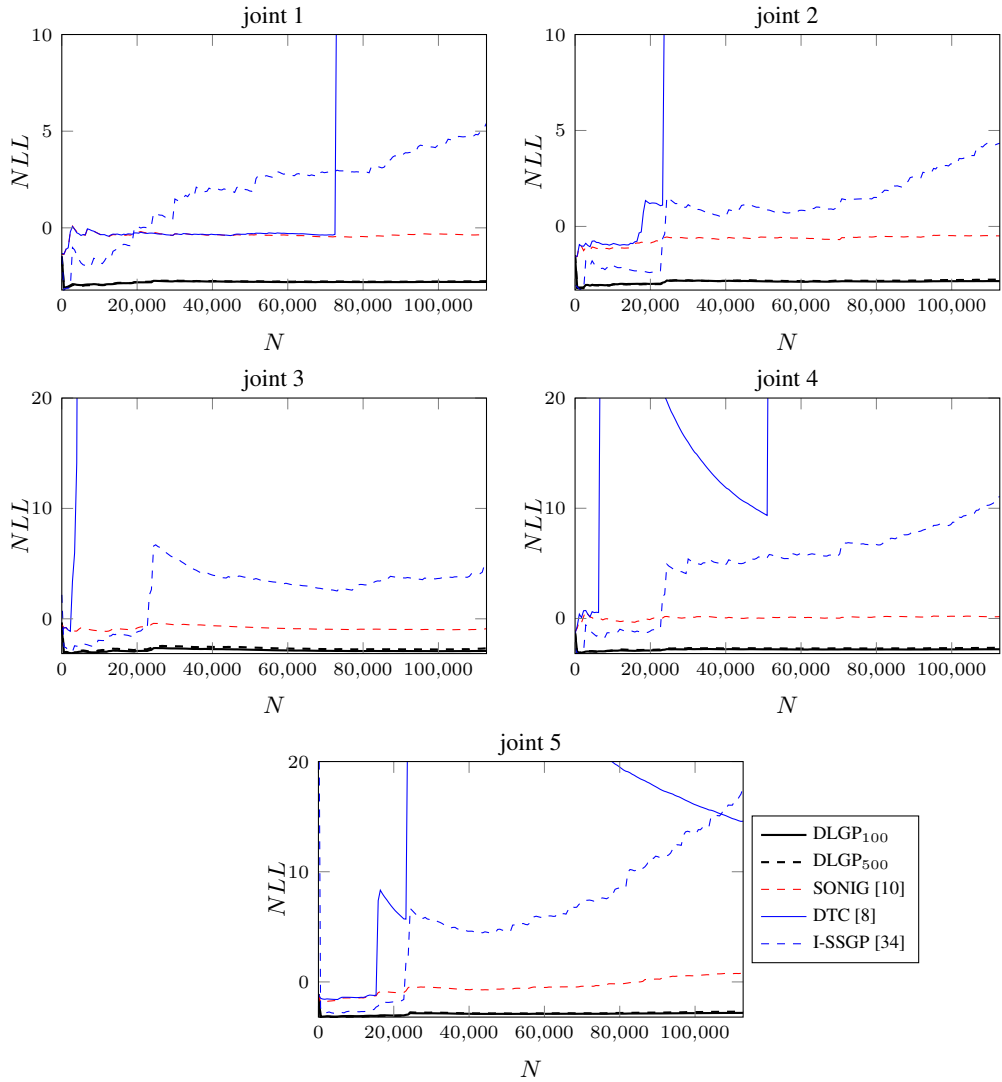


Figure 15: Average online negative log-likelihood for all joints of the KUKA flask pushing data set: environmental changes causing steps in the regression error lead to a significant deterioration of the reliability of the predictive distribution in state-of-the-art methods, while DLGPs are barely influenced.

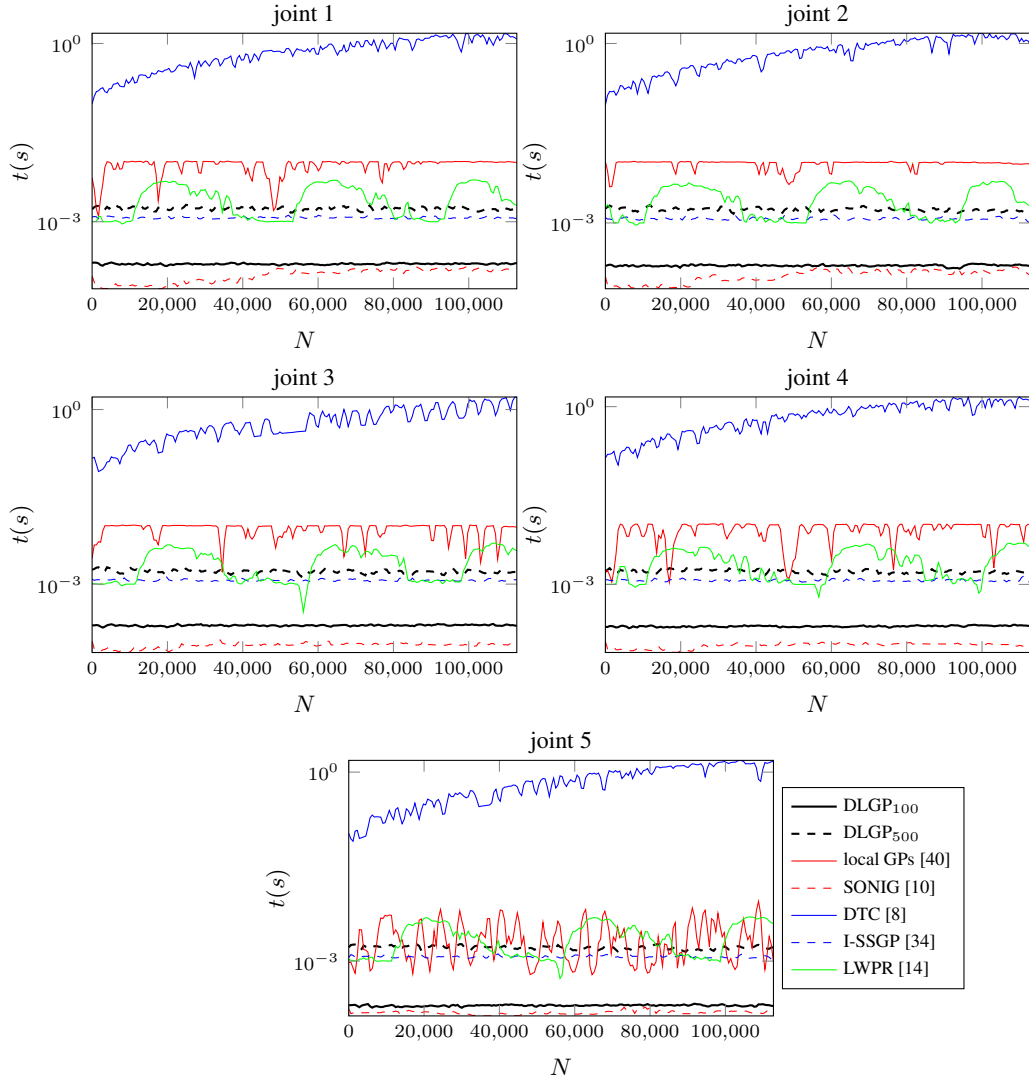


Figure 16: Average update time for all joints of the KUKA flask pushing data set: despite of large training set sizes, training of the DLGP_{100} model is faster than methods with a comparable regression performance.

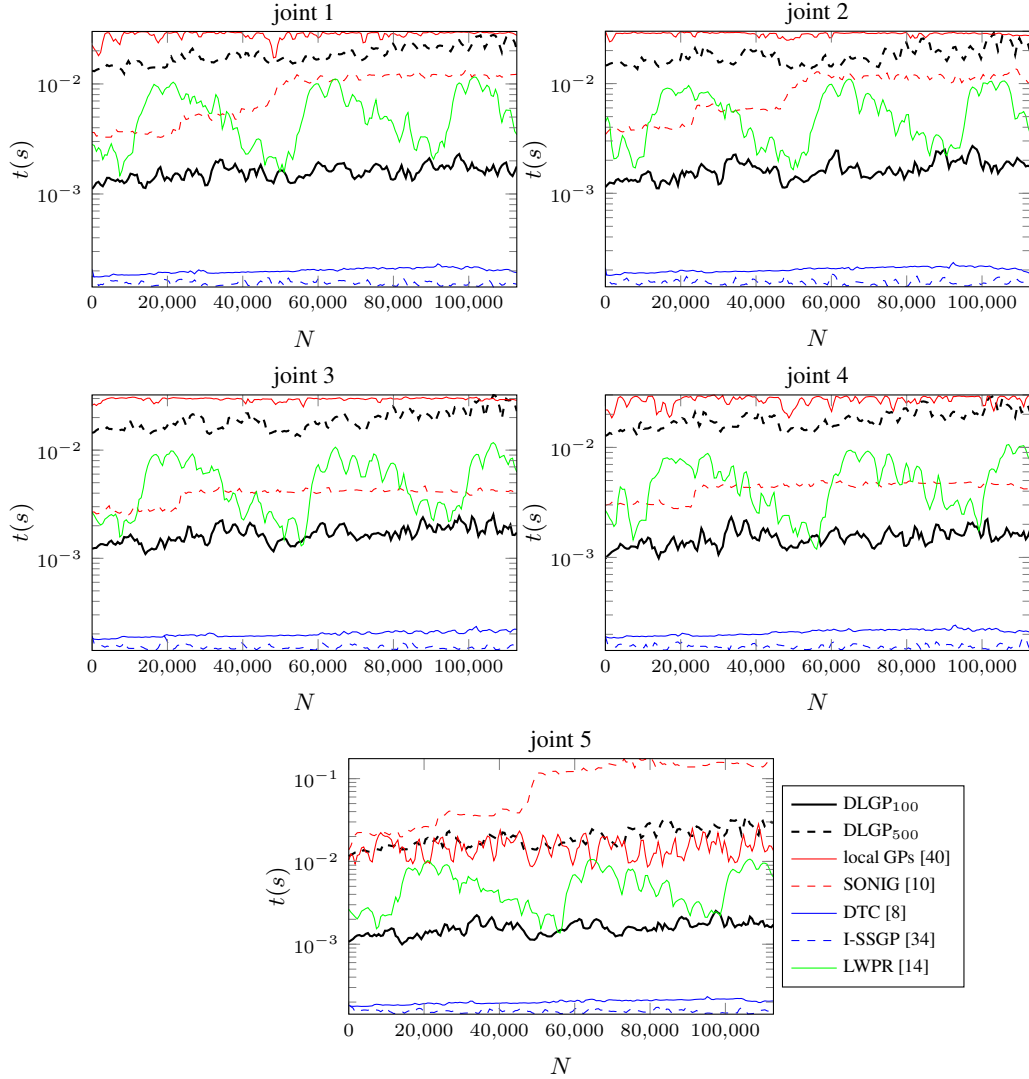


Figure 17: Average prediction time for all joints of the KUKA flask pushing data set: Even with variance prediction, DLGPs are only slightly slower than the fastest state-of-the-art method, and exhibit a prediction time to the commonly used LWPR.